Title

Substrate topography guides pore morphology evolution in nanoporous gold thin films

Authors

Chapman, Christopher AR

Daggumati, Pallavi

Gott, Shannon C

et al.

Publication Date

2016

DOI

10.1016/j.scriptamat.2015.07.039

Peer reviewed

Substrate Topography Guides Pore Morphology Evolution in Nanoporous Gold Thin Films

Christopher A.R. Chapman, Pallavi Daggumati, Shannon C. Gott, Masaru P. Rao, Erkin Seker

PII: S1359-6462(15)00330-9
DOI: doi:10.1016/j.scriptamat.2015.07.039
Reference: SMM 10751

Published in: *Scripta Materialia*

Received date: 19 June 2015
Revised date: 22 July 2015
Accepted date: 28 July 2015

Cite this article as: Chapman CAR, Daggumati P, Gott SC, Rao MP, Seker E, Substrate Topography Guides Pore Morphology Evolution in Nanoporous Gold Thin Films, *Scripta Materialia*, doi:10.1016/j.scriptamat.2015.07.039

Substrate Topography Guides Pore Morphology Evolution in Nanoporous Gold Thin Films

Christopher A. R. Chapman[a], Pallavi Daggumati[b], Shannon C. Gott[c], Masaru P. Rao[c,d,e], and Erkin Seker[b,*]

[a]*Department of Biomedical Engineering, University of California - Davis, Davis, CA 95616, USA*
[b]*Electrical & Computer Engineering, University of California - Davis, Davis, CA 95616, USA*
[c]*Department of Mechanical Engineering, University of California - Riverside, Riverside, CA 92521, USA*
[d] *Department of Bioengineering, University of California - Riverside, Riverside, CA 92521, USA*
[e] *Materials Science and Engineering Program, University of California - Riverside, Riverside, CA 92521, USA*

**Corresponding author: eseker@ucdavis.edu*

Abstract. This paper illustrates the effect of substrate topography on morphology evolution in nanoporous gold (np-Au) thin films. One micron-high silicon ridges with widths varying between 150 nm to 50 µm were fabricated and coated with 500 nm-thick np-Au films obtained by dealloying sputtered gold-silver alloy films. Analysis of scanning electron micrographs of the np-Au films following dealloying and thermal annealing revealed two distinct regimes where the ratio of film thickness to ridge width determines the morphological evolution of np-Au films.

Keywords: nanoporous material; annealing; dealloying; fracture; microfabrication

Nanoporous gold (np-Au), produced by selective dissolution of silver from a gold-silver alloy (known as *dealloying*) [1], is an emerging material that exhibits many desirable properties, including high electrical conductivity [2, 3], catalytic activity [4, 5], tunable pore morphology [3, 6-8], and compatibility with conventional micropatterning techniques [2, 3, 9, 10]. These properties translate into various applications, including multifunctional biomedical device coatings [2, 11, 12], bioanalytical sensors [13-15], catalytic applications [4, 5], as well as fundamental studies of structure-property relationships [10, 16-20]. As precise control of material morphology (e.g., pore size) is essential for these applications, it is necessary to have an understanding of parameters that influence morphology evolution. To that end, previous studies have explored the effect of alloy composition [17], dealloying method [21, 22], and post-processing techniques [6] on pore morphology. However, the effect of substrate topography on morphology evolution still remains largely unknown. As np-Au thin films supported on substrates benefit from the versatility of micropatterning (e.g., photolithography) and deposition techniques (e.g., physical vapor deposition, electroplating) for integration with devices, the role of substrate topography becomes increasingly important. The objective of this paper is therefore to address this knowledge gap by systematically investigating

the role of surface topography in morphology evolution. Specifically, we employed microridge arrays (MRAs) of textured silicon substrates coated with sub-micron-thick np-Au films for studying morphological evolution of np-Au films on multiple ridge widths and a smooth (non-textured) surface on a single chip (Figure 1).

Silicon MRAs were fabricated by photolithographic patterning with a deep ultraviolet (DUV) stepper (PAS 5500/300, ASML), followed by pattern transfer to the underlying silicon substrate with fluorine-based dry etching (SLR 770 ICP, Unaxis), and finally photoresist (PR) removal by oxygen plasma (PE-IIA, Technics). A portion of the chip was not patterned to serve as a smooth control surface, labeled as *blank* (Figure 1). Ridge profile and groove depth were characterized by cross-sectional images of test MRAs obtained by sectioning the chips with a focused ion beam system (CrossBeam XB1540, Carl Zeiss) and imaging them with a scanning electron microscope (SEM) (SUPRA 55, Carl Zeiss), as previously described [23]. The MRA fabrication process yields excellent agreement between the dimensions of expected and fabricated ridges [23]. Np-Au films were prepared as described previously [9]. Briefly, the silicon MRAs were cleaned by 10 minute-long immersion in a freshly prepared Piranha solution, composed of 1:4 volumetric ratio of hydrogen peroxide (30%) to sulfuric acid (96%). The array chips were subsequently rinsed in deionized (DI) water and dried under nitrogen flow prior to metal deposition with a magneto-sputtering system (Kurt J. Lesker). First, a 160 nm-thick chrome layer was sputtered to promote adhesion between the silicon substrate and the subsequent metallic layers. Next, 80 nm-thick seed layer of gold was sputtered and finally silver and gold were co-sputtered from different targets to obtain a 600 nm-thick alloy layer. All depositions were performed successively (without breaking the vacuum) in argon at a pressure of 10 mTorr. The composition of the alloy was 64% Ag and 36% Au (at. %) as determined by X-ray energy dispersive spectroscopy (Oxford Instruments). The samples were dealloyed in 70% nitric acid at 55 °C for 3 minutes and additional 12 minutes (total dealloying time of 15 minutes) to produce the np-Au films. In order to assess the effect of annealing on the pore area evolution, dealloyed chips were thermally treated for 3 minutes at 325 °C in a rapid thermal annealer (Accu Thermo 610).

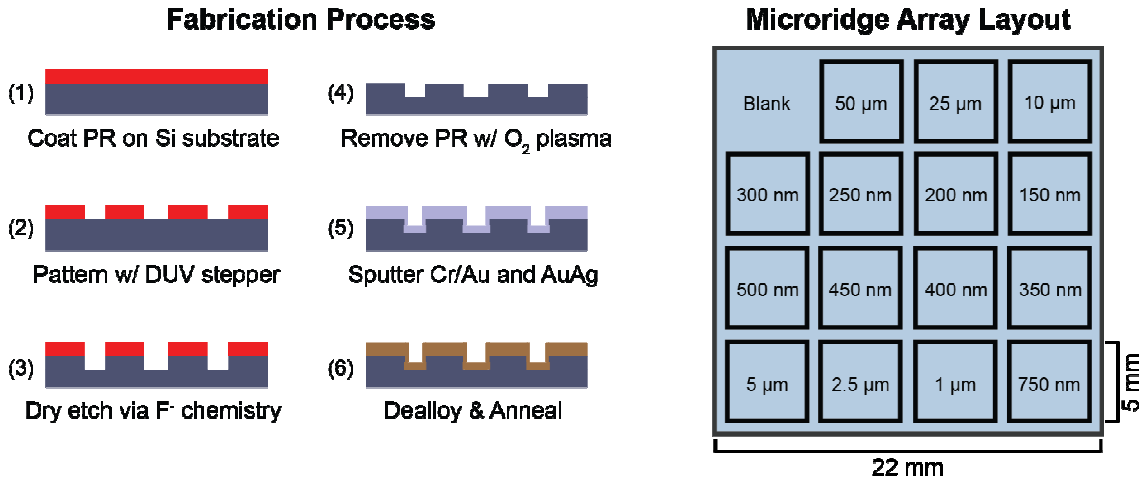

Figure 1. Summary of microfabrication steps for producing the silicon MRAs used as a substrate for np-Au thin film deposition. Each square region is covered by parallel ridges of equal width and spacing with the superimposed dimension.

The np-Au film morphology on the ridges was acquired with a SEM (Nova NanoSEM430, FEI) following three steps during np-Au processing: three minutes of dealloying, additional 12 minutes of dealloying, and three minutes of annealing at 325 °C. The SEM images (image field of 2.5 µm by 3 µm) were analyzed with custom ImageJ (National Institutes of Health shareware) scripts to obtain the areas of each void (i.e., pores and cracks). Briefly, each image was segmented to differentiate between pores/cracks (dark) and ligaments (light) in the images (Figure 2 and Supplementary Material) [9]. The cracks were defined as the surface features in top 5% of the pore area distributions for each case (Figure S1-S3). SEM images from three different regions on each ridge width, away from the ridge edges, were analyzed to calculate the median pore area/crack size (data point) and the corresponding standard error (error bar). The percent lateral shrinkage in the np-Au films on the ridges with respect to the initial width of the alloy were calculated from the low-magnification SEM images of the films on ridges (Figure 2 insets). Details of the fabrication and characterization methods can be found in the Supplementary Material.

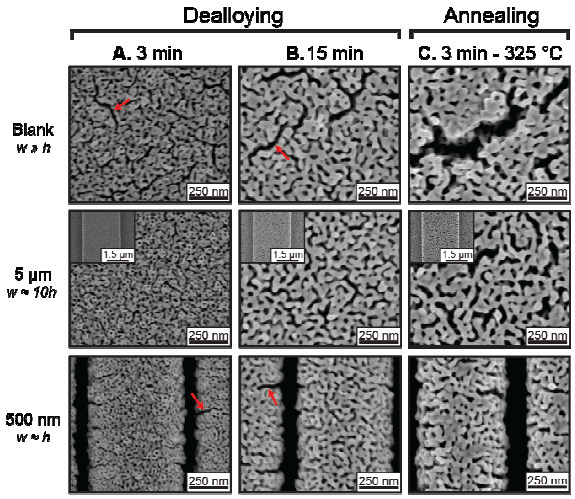

Figure 2. SEM images illustrating morphology evolution in np-Au films on three representative surface topographies after dealloying (A & B) and annealing (C). Relationship between film thickness, *h*, and the ridge width, *w*, dictates the nature of pore coarsening and crack formation. Initial crack formations during dealloying are highlighted by red arrows. The insets are low-magnification images of the films on 5 µm-wide ridges.

The underlying mechanism that leads to the open-pore morphology of np-Au with interconnected ligaments is the interplay between two processes: (i) roughening driven by dissolution of silver from the alloy, and (ii) smoothing/coarsening driven by enhanced surface diffusion of gold atoms at the metal-electrolyte interface [1]. After the three-minute dealloying, the np-Au films displayed smaller pore areas on each ridge (Figure 2A) in comparison to the typical dealloying time of 15 minutes (Figure 2B). It is expected that the short dealloying duration is sufficient for silver dissolution and porosity formation, but not long enough to produce significant surface diffusion-driven coarsening [8]. After the 15-minute dealloying, differences in pore morphologies for each ridge width became more apparent. Pore areas on both 5 µm and 10 µm ridges (also on the

blank to a lesser extent) became significantly increased (Figure 3A), compared to all other ridge widths. The np-Au-coated MRAs were then annealed at 325 ˚C for three minutes to enhance surface-diffusion of gold atoms, which is typically used for obtaining coarser morphologies [6, 7]. As for the case of dealloyed samples, the pore areas on 5 μm and 10 μm ridges as well as the *blank* control surface (denoted as ∞) remained much larger (~2x) than the narrower ridges (Figure 2 and 3A). Two regimes of pore morphology evolution with respect to ridge width become visible (Figure 2A). Below a *critical width* positioned between ridge widths of 1 μm and 2.5 μm, pore evolution is hindered (~2x increase from 3-min dealloying to annealing). Above this transition width, more significant pore coarsening (~4x increase for 5 μm and 10 μm, 3x increase for *blank*) is present. This is attributed to np-Au thin film mechanics in relation to the ratio of film thickness, *h*, to ridge width, *w*, which will be discussed later in the context of additional morphological and geometric phenomena.

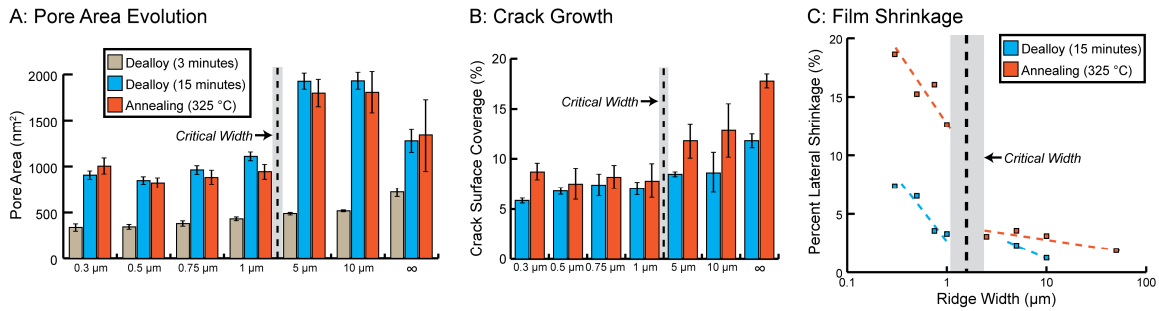

Figure 3. Below a *critical width* positioned at a ridge width between 1 μm and 2.5 μm, (A) pore coarsening is hindered, (B) crack surface coverage is suppressed, and (C) lateral film shrinkage is enhanced. Data points in all plots represent median values of measurements and the error bars represent the standard error.

Another important morphological phenomenon is the evolution of cracks, for which the two regimes persist. Generally, below the *critical width*, the percent crack surface coverage remained constant after both the 15 minute-dealloying and annealing steps, while crack coverage increased monotonically for ridges above the *critical width* and the *blank* surface (Figure 3B and Figure S1-S3). Both dealloying and annealing lead to tensile stress accumulation in np-Au films, which partially contributes to the presence of cracks in thin films as studied by others [24, 25]. While the chrome and gold adhesion layers make delamination of the precursor AuAg alloy (thereby its contribution to initial crack formation) unlikely, the grain boundaries of the AuAg alloy (as shown in Figure S4) may facilitate the formation of the hairline cracks early in the dealloying step. It is important to note that the crack widths (especially after annealing) are too large to be explained simply by stress relaxation through film cracking [10]. For example, for the case of blanket films (on *blank*), it is more probable that the tensile stress rapidly surpasses low tensile strength of the np-Au network (~12 MPa [26]), leading to formation of short hairline cracks after the 3-minute dealloying (Figure 2). The macroscopically-brittle nature of np-Au has been previously reported [18]. The small hairline cracks separated further during the subsequent processing steps leading to many randomly-oriented wide cracks (10s of nanometers) due to biaxial nature of the tensile stress (Figure 2). On the other hand, the cracks were localized at the edge of the ridges for

narrow ridge widths ($w \approx h$) and perpendicular to the ridges, as to be expected from the uniaxial tensile stress accumulation along the length of the ridge (Figure 3B). This, in turn, reduced the surface coverage of cracks for the narrow ridges.

A geometric evolution, *percent shrinkage*, is helpful in explaining the observed morphological phenomena. It has been reported by Seker *et al*. and others that np-Au experiences volume reduction during dealloying and annealing, although the underlying mechanisms are not fully understood [10, 18-20]. This volume reduction translates into tensile stress for mechanically-constrained films, such as substrate-supported np-Au in this study or freestanding double-clamped np-Au beams [18]. As ridge width decreased, the np-Au films exhibited more lateral shrinkage (with respect to the width of the deposited alloy) compared to the wider ridges (Figure 3C). Taken together with the observations of hindered pore coarsening (Figure 3A) and reduced crack coverage (Figure 3B) occurring for ridges below the *critical width*, it is suggested that the small ridges ($w \approx h$) impose less mechanical constraint on the thin film, since the film can contract laterally (Figure 4A). This is attributed to the reduced aspect ratio of np-Au (due to ridge width approaching film thickness) allowing for annealing-based tensile stress to translate into lateral film deformation (Figure 3C), thereby hindering pore coarsening (Figure 3A), as was also observed for freestanding np-Au cantilevers [18]. Above the *critical width*, the percent shrinkage is minimal (Figure 4B). For these substrates, the tensile stress accumulation leads to randomly-oriented hairline cracks away from the ridge edges that expand into large crack-like voids during additional dealloying and annealing (Figure S5). These cracks in effect create np-Au semi-islands with characteristic widths (1-5 μm) that are comparable to the narrow ridges below the *critical width*. The film's freedom to deform laterally, in turn, somewhat reduces the extent of pore growth, as observed for *blank* after annealing (see the condensed pores along the crack in Figure 2 and lower median pore area in Figure 3B). The intermediate ridge widths (such as 5 μm and 10 μm in this experiment) exhibit a similar, yet less pronounced, behavior to the np-Au on *blank*, where they exhibit coarsened pores (Figure 3A) but with less crack coverage (Figure 3B), because the aspect ratio is still not as large as the *blank*. The wider ridges (e.g., 5 μm) capture the key morphological and geometric manifestation of both the biaxial and uniaxial stress experienced as a function of ridge width (Figure S5) and serve as an excellent model to summarize the results (Figure 4). Within a micron-wide band along the edges of the np-Au film, pore growth is hindered due to unilateral shrinkage and perpendicular cracks are present reminiscent of uniaxial stress in narrow ridges (characteristic to Regime 1). Moving from the edge to the ridge midline, cracks become disordered and coarser pores are observed (characteristic to Regime 2).

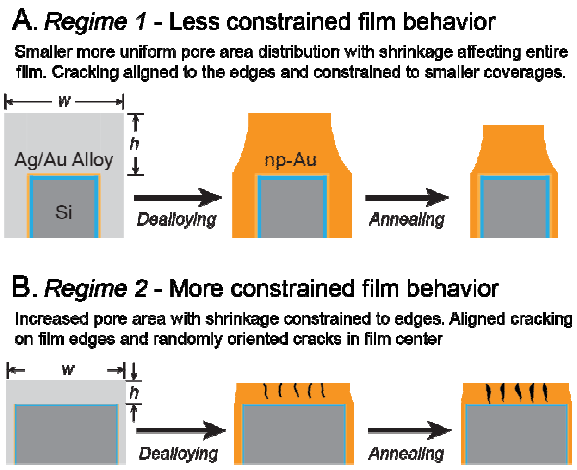

Figure 4. Schematic summary of the proposed regimes of thin film behavior that summarize the np-Au morphology evolution following dealloying and annealing steps.

We have demonstrated that np-Au morphology evolution is highly influenced by topography of the underlying substrate. As micropatterned np-Au thin films are gaining increasing use in device applications, we expect this study to inform researchers on design considerations for creating micron-scale np-Au films with desirable pore morphologies. To that end, the results suggest that micropattern widths that are within an order of magnitude of the film thickness should produce tunable pores with less cracking. In addition, the findings propose a novel technique to create different pore morphologies on a single chip by leveraging principles of basic thin film mechanics. Consequently, this approach circumvents batch-to-batch processing variability associated with using different samples and allows for parallel production and characterization of multiple thin film geometries, opening the door to high-throughput combinatorial study of structure-property relationships of other nanoporous metal systems.

We gratefully acknowledge the support from UC Lab Fees Research Program Award [12-LR-237197], Research Investments in the Sciences & Engineering (RISE) Award, and the National Science Foundation [1512745]. C. Chapman was supported by a National Science Foundation Graduate Research Fellowship [DGE-1148897] and a predoctoral fellowship from the National Institute of Health [T32-GM008799]. S. Gott was supported by a National Science Foundation Graduate Research Fellowship.

[1] J. Erlebacher, M. Aziz, A. Karma, N. Dimitrov, K. Sieradzki, Nature, 410 (2001) 450-453.
[2] E. Seker, Y. Berdichevsky, M. Begley, M. Reed, K. Staley, M. Yarmush, Nanotechnology, 21 (2010) 125504.
[3] T.S. Dorofeeva, E. Seker, Nano Research, 8 (2015) 2188-2198.
[4] T. Fujita, Guan, P., McKenna, K., Lang, X., Hirata, A., Zhang, L., Tokunaga, T., Arai, S., Yamamoto, Y., Tanaka, N., Ishikawa, Y., Asao, N., Yamamoto, Y., Erlebacher, J. & Chen, M., Nat. Mater., 11 (2012) 775-780.
[5] A. Wittstock, J. Biener, M. Bäumer, PCCP, 12 (2010) 12919-12930.
[6] L. Schade, S. Franzka, M. Mathieu, M.M. Biener, J.r. Biener, N. Hartmann, Langmuir, 30 (2014) 7190-7197.

[7] R. Li, K. Sieradzki, Phys. Rev. Lett., 68 (1992) 1168-1171.
[8] Y. Ding, Y. Kim, J. Erlebacher, Adv. Mater., 16 (2004) 1897-1900.
[9] P. Daggumati, Kurtulus, O., Chapman, C. A. R., Dimlioglu, D. & Seker, E., J. Visualized Exp., e50678 (2013).
[10] E. Seker, Reed, M. L. & Begley, M. R., Scripta Materialia, 60 (2008) 435-438.
[11] O. Kurtulus, Daggumati, P. & Seker, E., Nanoscale, 6 (2014) 7062-7071.
[12] C.A. Chapman, H. Chen, M. Stamou, J. Biener, M.M. Biener, P.J. Lein, E. Seker, ACS applied materials & interfaces, 7 (2015) 7093-7100.
[13] P. Daggumati, Matharu, Z. & Seker, E., Anal. Chem., (2015).
[14] J. Patel, L. Radhakrishnan, B. Zhao, B. Uppalapati, R.C. Daniels, K.R. Ward, M.M. Collinson, Anal. Chem., 85 (2013) 11610-11618.
[15] O. Shulga, D. Zhou, A. Demchenko, K. Stine, The Analyst, 133 (2008) 319-322.
[16] N. Senior, R. Newman, Nanotechnology, 17 (2006) 2311-2316.
[17] T. Fujita, L. Qian, K. Inoke, J. Erlebacher, M. Chen, Appl. Phys. Lett., 92 (2008) 251902-251904.
[18] E. Seker, Gaskins, J. T., Bart-Smith, H., Zhu, J., Reed, M. L., Zangari, G., Kelly, R. & Begley, M. R., Acta Materialia, 55 (2007) 4593-4602.
[19] S. Parida, D. Kramer, C. Volkert, H. Rösner, J. Erlebacher, J. Weissmüller, Phys. Rev. Lett., 97 (2006) 35504-35506.
[20] K. Kolluri, M.J. Demkowicz, Acta Mater., 59 (2011) 7645-7653.
[21] L. Qian, M. Chen, Appl. Phys. Lett., 91 (2007) 083105-083107.
[22] E. Detsi, M. Van de Schootbrugge, S. Punzhin, P. Onck, J. De Hosson, Scripta Mater., 64 (2011) 319-322.
[23] P. Vandrangi, S.C. Gott, R. Kozaka, V.G. Rodgers, M.P. Rao, PLoS ONE, 9 (2014) e111465.
[24] Y. Sun, K. Kucera, S. Burger, T. John Balk, Scripta Mater., 58 (2008) 1018-1021.
[25] O. Okman, D. Lee, J.W. Kysar, Scripta Mater., 63 (2010) 1005-1008.
[26] T.J. Balk, C. Eberl, Y. Sun, K.J. Hemker, D.S. Gianola, JOM, 61 (2009) 26-31.

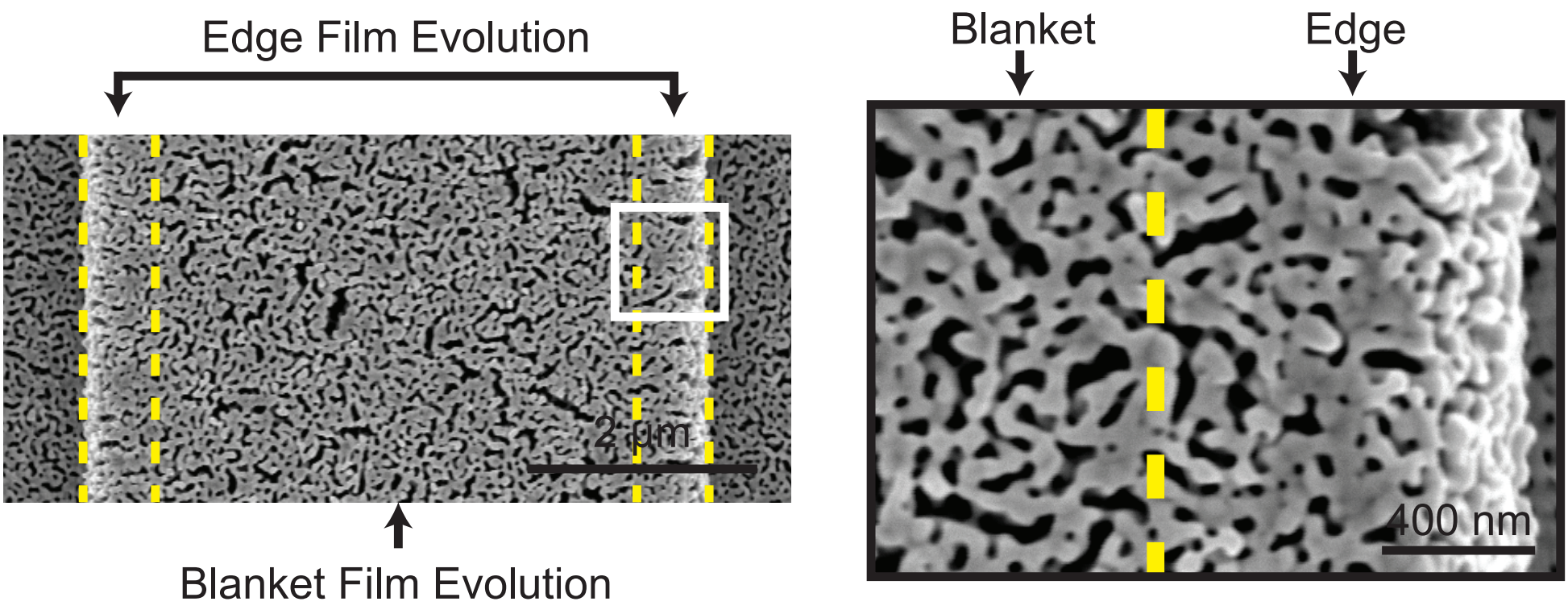
Edge Film Evolution
2 μm
Blanket Film Evolution
Blanket
Edge
400 nm